ACS APPLIED MATERIALS & INTERFACES

Research Article

www.acsami.org

First Step into Space: Performance and Morphological Evolution of P3HT:PCBM Bulk Heterojunction Solar Sells under AM0 Illumination

Shuai Guo,[†] Christian Brandt,[‡] Thomas Andreev,[‡] Ezzeldin Metwalli,[†] Weijia Wang,[†] Jan Perlich,[§] and Peter Müller-Buschbaum*,[†]

[†]Technische Universität München, Physik-Department, Lehrstuhl für Funktionelle Materialien, James-Franck-Strasse 1, 85748 Garching, Germany

[‡]Airbus Defence and Space, BD Equipment, Robert Kochstrasse 1, 85521 Ottobrunn, Germany

[§]Deutsches Elektronen-Synchrontron (DESY), Notkestrasse 85, 22603 Hamburg, Germany

ABSTRACT: P3HT (poly(3-hexylthiophene-2,5-diyl)):$PC_{61}BM$ ([6,6]-phenyl-C61 butyric acid methyl ester) bulk heterojunction solar cells are fabricated and characterized as a function of solar intensity, temperature, and aging at vacuum conditions under illumination with AM0 illumination for testing potential use in space applications. The evolution of the inner film morphology is probed with grazing incidence X-ray scattering techniques and correlated with the evolution of the efficiency during aging. Grazing incidence wide-angle X-ray scattering shows almost no change of the crystalline structure of the P3HT:PCBM films due to aging. In contrast, the morphological evolution on the mesoscale extracted from grazing incidence small-angle X-ray scattering can explain the observed decay of the overall efficiency. The behavior at high solar intensities as well as elevated temperatures suggests that organic solar cells have high potential for space applications in the future.

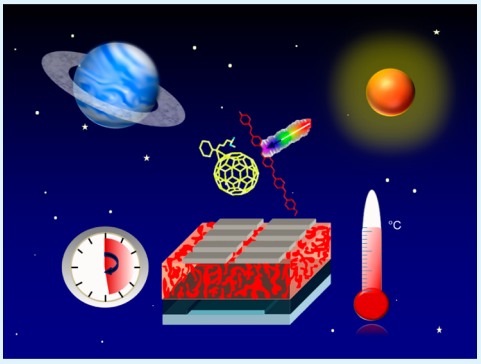

KEYWORDS: *organic photovoltaics, solar intensities, aging, nanomorphology, GISAXS, GIWAXS*

1. INTRODUCTION

Polymer solar cells have been undergoing rapid development both in academy and in industry during the past years.[1−10] Although significant efforts have been put forward on the improvement of the device performance for the application in a terrestrial framework, results showing the potential for space applications are rather scarce.[11,12] In the case of solar generators for space applications, two factors are dominating the technology selection process: the power/mass ratio and the volume of the device.[13,14] Despite the fact that at the moment all space solar cells are inorganic-based devices, the advances in polymer-based solar cells render them promising candidates because, e.g., polymer-based solar cells are extremely light-weight as compared with the traditional inorganic solar cells. Polymers mainly consist of light atoms (H_1^1 and C_6^{12}), which makes them superior to traditional semiconductors (Si_{14}^{28} or $Ga_{31}^{70}As_{33}^{75}$) in terms of weight. In addition, due to their special properties, polymer molecules tend to form less dense structure compared with traditional semiconductors which contain densely packed crystalline structures. Thus, the advantage for space applications is not only a possible low-cost production of the solar cell itself, but also the extremely light weight compared to traditional solar cells, allowing them to be mounted also on flexible lightweight substrates. In turn, this would mean that the overall solar array power can be brought into regions which are today not achievable as typical mechanical restrictions like moments of inertia or too complex deployments of panels would no longer be significant.

In this respect, for polymer-based solar cells, power conversion efficiencies (PCE) of up to 12% have been achieved recently,[15] which is a big step forward for this emerging class of solar cells to compete with the inorganic devices in space applications. The prospect of high-throughput module manufacture of organic photovoltaics by roll-to-roll printing method could render the cost of modules less than 1 euro/watts peak.[16] However, before the idea of polymer-based solar cells for space applications can become reality, the novel devices need to be systematically tested for such purposes. Testing conditions for terrestrial and space applications will differ significantly. Solar cells used for space power applications, like those on communications satellites or for other space missions, are generally characterized using solar spectrum AM0.[13,17,18] AM0 stands for air mass zero, which is typically used as the extraterrestrial solar spectral irradiance distribution, approximated by the 5800 K blackbody. In comparison, AM1.5 is universal when characterizing terrestrial solar panels. The main difference between these two spectra is the UV-light particularly included in the AM0 spectrum. In general, UV-light is potentially harmful for organic molecules and thus can

Received: July 14, 2014
Accepted: September 25, 2014
Published: September 25, 2014

enhance the degradation process of an organic solar cell device. As a consequence, the tolerance of polymer-based solar cells against strong solar irradiance containing UV-light, potentially high temperatures, and accumulated light illumination must be tested systematically. Moreover, if these initial tests are successful, the influence of high-energy particle radiation on the solar cells would need to be addressed in a second step.

In the present investigation we focus on the most intensively researched model system for polymer-based solar cells. The active layer of the solar cell is based on P3HT (poly(3-hexylthiophene-2,5-diyl)):$PC_{61}BM$ ([6,6]-phenyl-C61 butyric acid methyl ester) in a bulk heterojunction (BHJ) geometry.[19−24] As an initial investigation of the potential of such type of solar cells for possible space applications, we focus on the influence of different solar intensities, device temperatures, and the aging effect on the performance of P3HT:PCBM BHJ solar cells. From this investigation, fundamental conclusions concerning the usage of organic solar cells in future space solar panels are obtained. The polymer solar cells are characterized with AM0 spectrum, i.e., without the characteristic absorptions from the Earth's atmosphere, under different solar intensities, starting from 0.8 AM0 (107.83 mW/cm^2) to 3.3 AM0 (444.81 mW/cm^2), at room temperature. Moreover, a polymer solar cell is examined in a temperature range from 28 to 80 °C at 1.0 AM0 solar intensity. Moreover, the aging problem is addressed by measuring the device performance at room temperature as a function of time under 1.0 AM0. The aging effect is further investigated with the aid of advanced X-ray scattering techniques in order to understand the degradation mechanism on a molecular level up to the mesoscale. The X-ray scattering experiments combine GISAXS (grazing incidence small-angle X-ray scattering) and GIWAXS (grazing incidence wide-angle X-ray scattering). GISAXS allows for probing the buried inner film structure of the active layer on the mesoscale, which is essential in the BHJ geometry. In addition, GISAXS is a nondestructive probe which requires no special sample preparation.[25−28]

The crystal structure of the films, such as the lattice constants, the orientation of the crystals, as well as crystal size, are obtained with GIWAXS measurements.[29−32] The combination of the results from these X-ray scattering experiments with the characterization of the solar cells helps to address the correlation between the morphological evolution of the active layer and the solar cell efficiency.

2. EXPERIMENTAL SECTION

2.1. Device Preparations. P3HT (poly(3-hexylthiophene-2,5-diyl)) and $PC_{61}BM$ ([6,6]-phenyl-C61 butyric acid methyl ester) were purchased from Rieke Metal Inc. and Nano-C, respectively, and used as supplied. Each component was dissolved in 1,2-dichlorobenze separately and then mixed with a ratio of P3HT:$PC_{61}BM$ = 1:0.8 under ambient conditions. The final concentration of the solution was 60 mg/mL.

For the device fabrication, ITO-covered glass substrates were patterned with an adhesive film and chemically etched to avoid potential short circuits. The substrates were consecutively cleaned in alconox solution, ethanol, acetone, and isopropyl alcohol in an ultrasonic bath for 10 min, respectively. To increase the hydrophilicity of the ITO surface before spin-coating of the PEDOT:PSS (poly(3,4-ethylenedioxythiophene):poly(styrenesulfonate)) films, oxygen-plasma treatment was applied for 10 min. The PEDOT:PSS solution was spin-coated at 3000 rpm for 60 s, followed by spin-coating P3HT:$PC_{61}BM$ at 2000 rpm for 30 s. In between, all samples were annealed at 150 °C in air to remove residual water from the PEDOT:PSS film. As top contact a 100 nm aluminum layer was thermally evaporated under vacuum conditions (3.8×10^{-5} mbar) at a deposition rate of 20 Å/s. Finally, an annealing of the whole device was performed in nitrogen atmosphere (140 °C for 10 min). For each solar cell the effective device area was about 0.15 cm^2, determined by the overlapping area between the ITO and aluminum contacts. Finally, the as-prepared polymer solar cells were encapsulated with epoxy and glass. Transport of the devices to the Airbus Defense and Space laboratory for photoelectrical characterization occurred the day after preparation. To fit with the contacting needs of a sun simulator for space cells in the Airbus Defense and Space laboratory, each electrode was extended via a copper tape with an one-side conductive adhesive to perform the $I-V$ characterization.

2.2. Photovoltaic Characterization. All $I-V$ curves were measured with an AM0 spectrum, to which the solar cells would be exposed in an extraterrestrial application. Thus, the high-energy radiation in the ultraviolet region being typically removed by the Earth's atmosphere is still present in the spectrum. For each measurement one pixel of the solar cell was selected (typically for the ITO substrate size of 2.2×2.2 cm^2 used in present investigation), 8 pieces of mini solar cells (8 pixels of each solar cell) were fabricated, and different solar cells were probed for different measurements.

The used sun simulator is a self-developed steady-state three-source simulator, arranging the AM0 spectrum with a Xe high-pressure lamp and two halogen lamps. Spectral control is guaranteed by three different types of secondary working standards ($InGaP_2$, GaAs, and Ge) which are derived from primary standards having been calibrated by a balloon flight in space. All photoelectrical measurements were carried out with a four-wire technique in order to get rid of additional equipment resistances. For voltage and current measurement, a Keithley 2400 source meter has been used.

Measurements with Different Solar Intensities. First, polymer solar cells were characterized using different solar intensities. The measurements covered a range from 0.8 AM0 to 3.3 AM0 and were performed at room temperature. By controlling the short-circuit current of a monocrystalline silicon calibration cell, the different light intensities were realized by simply adjusting the distance between the solar cell and the light source of the solar simulator. Due to the small size of the solar cell, an intensity inhomogeneity can be neglected.

The ITO electrode was connected with two parallel wires with the plus pinholes and the aluminum electrode with minus pinholes. The solar intensity was set precisely to 0.8, 1.0, 1.2, 1.5, 2.0, 2.5, 3.0, and 3.3 AM0. Note that in the present work even the lowest chosen light intensity 0.8 AM0 is equal to a solar intensity of 107.304 mW/cm^2, which is still higher than the commonly used standard AM1.5G solar spectrum radiance (corresponding to 100 mW/cm^2). After these measurements with different solar intensities, the polymer solar cell was remeasured under 1 AM0 conditions. No efficiency decay was observed.

Measurements at Different Temperatures. A temperature range from 28 to 80 °C was selected, and measurements were performed at 1 AM0 solar intensity. The solar cell was placed horizontally on a heatable copper block. For temperature control a thermal sensor has been mounted next to the solar cell. By increasing the temperature of the copper block, the $I-V$ curves were recorded as soon as the desired temperature was reached. $I-V$ curves were measured at 28, 30, 35, 40, 45, 50, 55, 60, 65, 70, 75, and 80 °C.

Time-Dependent I−V Measurements. The time-dependent evolution of the solar cell performance was probed at room temperature under 1 AM0 at vacuum conditions of 10^{-5} mbar. The vacuum chamber was installed with a special glass window being transparent to UV-light. $I-V$ curves were recorded every few seconds over 30 min.

2.3. GISAXS/GIWAXS Measurements. For X-ray scattering experiments the P3HT: $PC_{61}BM$ solution was spin-coated on acid pre-cleaned silicon substrates instead of ITO substrates to reduce the background scattering caused by rough ITO surface.[33] As known from previous work, the characteristic lateral structures within the films are comparable for both substrates.[30,33] These samples were exposed to exactly the same light illumination and temperature conditions as corresponding solar cells (see description above).

Grazing Incidence Small-Angle X-ray Scattering. GISAXS measurements were performed at the synchrotron beamline BW4 of the DORIS III storage ring located in Hamburg, Germany.[34] Each sample was mounted on the sample holder of the instrument and aligned individually to the required geometry. An X-ray wavelength of 0.138 nm with a beam size of 23 × 36 μm^2 (generated by an assembly of refractive beryllium lenses) was used. All GISAXS measurements were performed at a shallow incident angle of 0.4°, which was set above the critical angle of both P3HT and $PC_{61}BM$. Therefore, structural information from both surface and inner film structures was probed. The scattered intensity was recorded with a two-dimensional (2D) MarCCD detector at a sample−detector distance of 2.11 m. Due to the applied instrumental settings, the resolution of the measurement was determined by the sample−detector distance. To avoid beam damage to the detector, a beam-stop was used to shield the high-intensity specular peak. In case of high diffuse scattering, a rod-shaped beam-stop was positioned in the center of the detector, which allowed for longer counting times and thereby enabled the observation of more structural details. To analyze the 2D GISAXS data, horizontal line cuts were performed at the critical angle of P3HT or PCBM. These horizontal line cuts contain information about lateral structures as well as spatial structural correlations. Modeling of the intensity distribution of the horizontal line cuts was done in the framework of the so-called effective surface approximation within the distorted wave Born approximation (DWBA). From this modeling, prominent in-plane structures are detected.[35]

Grazing Incidence Wide-Angle X-ray Scattering. GIWAXS measurements were performed at the same beamline with similar instrumental settings. Compared with the GISAXS geometry, the sample−detector distance for GIWAXS was decreased to 121 mm to probe smaller structures related to the crystalline part of the films. Moreover, the incident angle was set as 0.2° to avoid background from the substrate.

3. RESULTS AND DISCUSSION

In the present investigation we focus on several parameters providing information about the usability of P3HT:$PC_{61}BM$-based solar cell in space application. Based on the AM0 solar spectrum, we perform a systematic investigation on the influence of the solar intensity and the effect of elevated temperatures. Moreover, we look into initial aging of the polymer solar cells.

3.1. Device Performance at Different Solar Intensities.

Based on the AM0 spectrum, the solar intensity was varied from 107.83 to 444.81 mW/cm^2 to explore the effect of illumination with different intensities on the device performance of the organic photovoltaic devices. Such increase in solar intensity would happen in space applications which have orbits closer to the sun than our Earth. So far in literature, polymer solar cells are routinely investigated with the AM1.5 spectrum only.[36,37] High solar intensities, such as realized in concentrator cells' arrangements, as well are based on the AM1.5 spectrum only.[38−40] Due to the differences in the spectrum, it remains unclear to what extent such investigations can be transferred to potential space applications.

In Figure 1, an exemplary plot of current−voltage (I−V) curves as a function of solar intensity under the AM0 spectrum at 28 °C is presented.

At first glance the curves show a clear current increase with light intensity and an additional voltage increase. For the higher measured voltages, the change of the steepness with increasing light intensity indicates that the effect of the cell series resistance is getting pronounced. In this context it is worth mentioning that dark I−V curves (not shown here from the studied cells) fit well to the two-diode model equations. Also by these fits a notable series resistance has been found to be in order to cause this effect. This is not obvious as the solar cell grid is not optimized for such high light intensities. As mentioned in the experimental part, additional resistances due to contacting issues can play also a role.

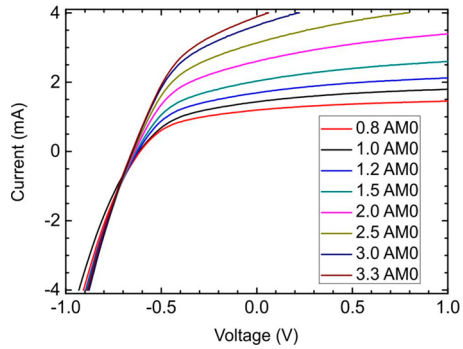

Figure 1. Exemplary plot of current−voltage curves measured with increasing solar intensity under the AM0 spectrum at 28 °C.

The corresponding characteristic photovoltaic device parameters from the I−V curves in Figure 1, open-circuit voltage V_{oc}, short-circuit current I_{sc}, fill factor FF, and efficiency η as a function of the solar intensity P_{light}, are shown in Figure 2.

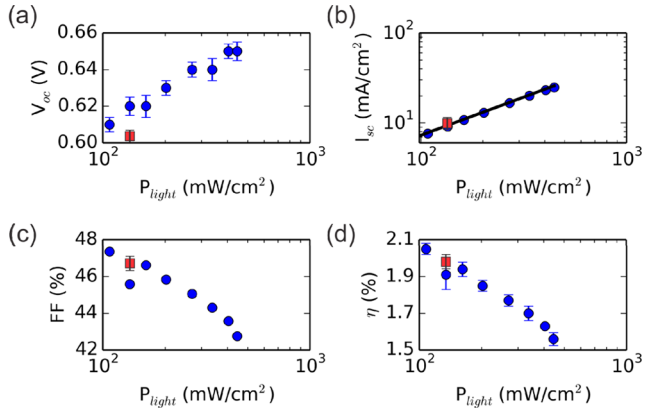

Figure 2. Device characteristics expressed in (a) open-circuit voltage V_{oc}, (b) short-circuit current I_{sc}, (c) fill factor FF, and (d) efficiency η, plotted as a function of solar intensity of the AM0 spectrum at 28 °C (blue dots). After the characterization with different solar intensities, the cell is remeasured (red square). A fit of the power-law dependence between I_{sc} and incoming light P_{light} is indicated as a black line in diagram (b).

Despite nonoptimized efficiency, it is very important to first understand on a more fundamental level the light/efficiency relationship. V_{oc} and I_{sc} increase with increasing solar intensity range, whereas FF and η decrease. Such general behavior is in agreement with observations on polymer:fullerene system using AM1.5 spectrum and concentrator setups.[37−42] As a consequence, the change in spectrum illuminating the solar cells does not change the general trend. In other words, the gradual increase of V_{oc} suggests that V_{oc} is not only determined by internal factors such as work function difference of the donor and acceptor materials, but also by external factors such as the solar intensity. The increase in V_{oc} with increasing solar intensity is also observed in traditional semiconductor solar cells;[43] however, the mechanism responsible for this increase in organic solar cells is still under debate.

In Figure 2b the short-circuit current as a function of solar intensity is displayed in a double-logarithmic presentation. The higher amount of photoinduced charge carriers generated with increasing light intensity explains this observed I_{sc} increase. In semiconductor cells this increase follows a linear behavior even up to light concentrations higher than 100 AM1.5. For the studied polymer cells, the I_{sc} increase is found to follow a power-law dependence $I_{sc} = P_{light}^{\alpha}$, with $\alpha = 0.83$, which identifies the type of charge loss mechanism in a typical P3HT:PCBM BHJ solar cell. In literature generally two types of charge recombination mechanisms are discussed: monomolecular and bimolecular recombination. Monomolecular recombination suggests that the free negative and positive charge carrier recombine on the same molecule, while the situation that the free charge carriers reside on two different molecules and then recombine with each other represents the bimolecular recombination. For pure bimolecular recombination, I_{sc} is supposed to follow a square-root relation with the P_{light}, that is, $\alpha = 0.5$. Since we find a different exponent for the power-law, we concluded that the main charge-carrier losses in our solar cell under the AM0 spectrum are monomolecular recombinations. With respect to the total device efficiency, however, the gradual decrease of the FF of the polymer solar cells as a function of increasing solar intensity overtakes the increase of V_{oc}*I_{sc}. As a consequence the probed values of η drops. As mentioned in the discussion of Figure 1, the found electrical behavior of this polymer cells is diode-like. According to the given argumentation, one possible governing mechanism responsible for this efficiency drop is related to a nonoptimized cell grid design, which results in detrimental effects from the cell series resistance at high light intensities. Based on AM1.5 spectrum, such behavior was reported by Tromholt et al. for inverted device architecture (system glass/ITO/ZnO/P3HT:PCBM/PEDOT:PSS/Ag).[42]

After these measurements with different solar intensities, the same polymer solar cell is remeasured under 1 AM0 conditions. The solar cell efficiency stays unchanged within the experimental error bars as shown in Figure 2d.

In summary, it can be stated for the light spectrum/light intensity behavior that the studied polymer solar cells are fully capable to operate under the spectra present in space. It can be also concluded that polymer solar cells are even functional at light intensities, which are significantly higher than the ones on Earth.

3.2. Device Performance at Different Temperatures. In practical space application, the temperature of the solar cell cannot be kept constant at room temperature under long-term solar irradiation, which makes the investigation of the temperature response of polymer solar cells imperative.

As seen in Figure 3a, V_{oc} decreases gradually with increasing temperature when illuminated with the AM0 light spectrum. This behavior agrees with observations using AM1.5 radiation performed by Park et al.,[36] which reported a linear decrease of V_{oc} from 0.73 to 0.63 V from 200 K (−73.15 °C) to 350 K (76.85 °C). Also based on AM1.5 radiation, Katz et al. investigated the performance of MDMO-PPV:PCBM polymer solar cell under increased temperatures from 25 to 60 °C. For MDMO-PPV:PCBM polymer solar cell, the power conversion efficiency reached the highest value at a temperature of 50 °C due to the dual effect of increasing I_{sc} and decreasing V_{oc}.[44]

In our investigation with the AM0 spectrum, a similar trend is found for the P3HT:PC_{61}BM-based solar cell as shown in Figure 3: I_{sc} increases as a function of temperature, while V_{oc} decreases. It is suggested that the observed strong temperature dependence of I_{sc} is correlated with the electronic transport properties of the used materials. In an organic semiconductor device, the free charge carriers are transported in a typical hopping type and therefore are thermally activated.[45,46] After the step of exciton dissociation, charge transport occurs. A lowered increase of I_{sc} occurs when the temperature reaches 50 °C, which is suggested to be correlated with the morphology alternation of the active layer or the glass transition temperature (T_g) of the polymer P3HT.[47−49] As the temperature increases, the mobility of the polymer chains and therefore the mobility of free charge carriers increase, resulting in a simultaneous increase of I_{sc}, as shown in Figure 3b.

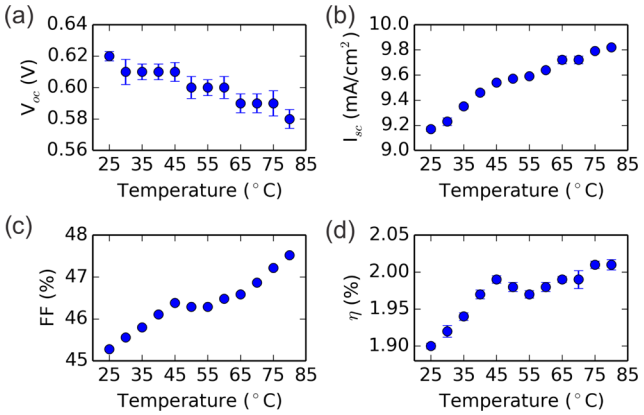

Figure 3. Device characteristics for P3HT:PC_{61}BM BHJ solar cells at constant 1 AM0 solar intensity: (a) V_{oc}, (b) I_{sc}, (c) FF, and (d) η plotted as a function of temperature.

Along with the higher current increase than voltage decrease with temperature, the curve fill factor and the cell efficiency are increasing as seen in Figure 3c and 3d. Peters et al. hypothesize that the degradation of the photoactive layer caused by photochemical reactions in polymer is responsible for the loss of V_{oc} during the initial burn-in stage.[49] The increasing trend of temperature-dependent FF can be explained by the deduced series R_s and the parallel resistances R_p while increasing the device temperature.[37] Nevertheless, details on the temperature increase of these cell parameters seem to be complex as the behavior is e.g. not linear.

All in all, the temperature dependent results reveal that the studied type of solar cell is capable to operate at typical geostationary orbit temperatures which can be up to 70 °C high. In contrast to conventional semiconductor space cells, the efficiency increases with temperature have a beneficial effect for space applications as in-orbit the solar cells are heated by the strong illumination.[50]

3.3. Aging of Solar Cells at AM0 Conditions. So far, we have focused on the effect of illumination with different solar intensities and temperature on the device characteristics of P3HT:PC_{61}BM BHJ solar cells at AM0 conditions. Although they show some promising trends for space applications, the overall limited lifespan of polymer solar cells must be taken into account. It was reported by Tipnis et al. that modules based on P3HT:fullerene BHJ solar cells have presented approximately 3 years of lifetime.[51] In general, polymer solar cells are complicated multilayer structures, and degradation can be caused by degradation of each component or chemical and physical interaction between layers. Several degradation mechanisms have been proposed in literature: photo-oxidation

and morphological degradation of the photoactive layer, atomic displacement, defect states, corrosion, and delamination of the contacts.[52−56] In the case of the investigated P3HT:$PC_{61}BM$ solar cells, degradation occurs under vacuum conditions as seen in Figure 4.

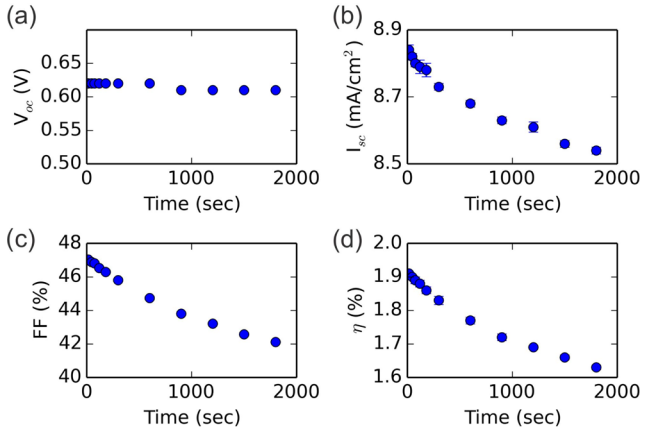

Figure 4. Device characteristics for P3HT:$PC_{61}BM$ BHJ solar cells under permanent illumination with 1 AM0 at constant temperature of 28 °C: (a) V_{oc}, (b) I_{sc}, (c) FF, and (d) η plotted as a function of time.

The values of I_{sc} and FF decrease clearly at longer exposure times whereas V_{oc} remains rather constant due to the absence of oxygen. Therefore, oxidization of the active layer or aluminum contacts is not the dominant mechanism for degradation in our study. Typically investigations on degradation of organic solar cells for terrestrial applications under solar spectrum AM1.5 have concluded that the presence of oxygen will oxidize the organic layer and aluminum electrode, and the localized moisture encroachment causes a dawdling degradation as well.[57,58] For space applications the absence of oxygen will rule out such problems. Recent studies on the effect of light-induced degradation suggest that an increased number of traps and p-type doping contribute to the decrease of I_{sc} in the first hours of illumination. Peters et al. reported a similar degradation on the same system as observed in our study with the potentially harmful UV radiation filtered out in their study.[59] From their results and our previous investigations on solar cell aging characterized under AM 1.5 spectrum conditions, a decreasing trend of the overall efficiency as a result of predominantly decreased FF and I_{sc} is observed.[49,56,59] In comparison, the solar cells subjected to the illumination AM0 spectrum in present work exhibit a similar overall "burn-in" efficiency loss primarily due to the decrease of FF and V_{oc}. Moreover, Tanenbaum et al. reported the lifetime and long-term stability of encapsulated P3HT:PCBM devices in the range of 0.5−40 h.[60]

To further explore the degradation mechanism, GISAXS measurements have been performed on samples exposed to 1.0 AM0 solar radiation for several illumination times. As a powerful method, GISAXS offers access to excellent statistics of the inner film morphology such as lateral structure size, size distribution, and spatial correlations. Information about lateral structures is extracted by performing horizontal line cuts at the Yoneda peak position of PCBM on the 2D GISAXS data and fitting these line cuts (shown in Figure 5) with a 1D paracrystal model within the frame explained in the experimental section. The resulting fitting parameters are shown in Figure 6. For

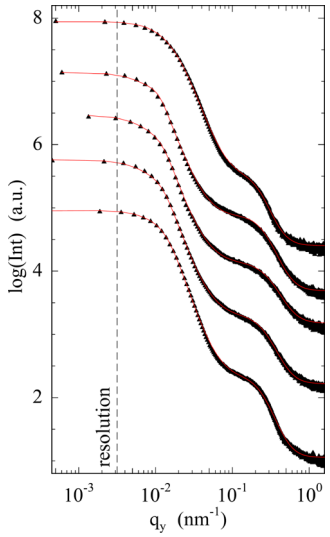

Figure 5. Exemplary horizontal line cuts (black triangles) of the 2D GISAXS data and the corresponding model-fitted curves (red lines) measured under permanent illumination with 1.0 AM0 at constant temperature of 28 °C. From bottom to top, the curve corresponds to the sample under illumination of 1, 300, 600, 900, 1800 s, respectively. All curves are shifted along the *y*-axis for the clarity of the presentation.

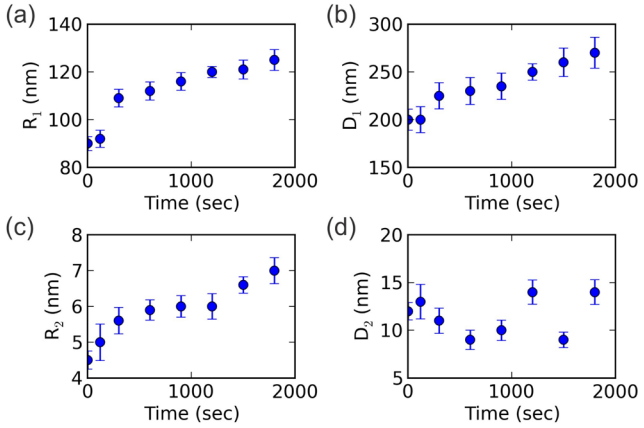

Figure 6. Characteristic structures extracted from modeling the horizontal line cuts of the 2D GISAXS data measured under permanent illumination with 1.0 AM0 at constant temperature of 28 °C: (a, c) form factors (domain size) R_1 and R_2 and (b, d) structure factors (distances) D_1 and D_2.

proper fitting of the GISAXS intensities, two distinct structures are required. Thus, the main characteristic parameters of the active layer are two mean object diameters R_1 and R_2 and the corresponding mean distances between two adjacent objects D_1 and D_2. It is observed that both object populations, small and large ones, grow in size under illumination. Moreover, the distances between the large objects grow, whereas the one between the small objects remain basically unchanged. The extracted smaller domain size R_2 is in agreement with the determined $PC_{60}BM$ cluster size of several nanometers from the investigation on BHJ P3HT:PC_xBM solar cells with GISAXS by Huang et al.[26]

As for the extracted larger domain size R_1, within the length scale of about 100 nm range, a growing PCBM domain size is observed with increasing illumination time, and the following scenario is suggested: The final large PCBM-rich domains (about 125 nm after 30 min illumination) are formed possibly

from the initially existing larger PCBM domains (of about 90 nm) or by PCBM molecules existing originally in the amorphous P3HT polymer matrix as suggested by Chen et al.[61] Additionally, it is observed that these increasing PCBM-rich domains, within the length scale of 100 nm, are effectively separated further apart (indicated as D_1), which can directly explain the decreased I_{sc} due to the reduced amount of interface between the P3HT and PCBM phases. This observation agrees with our real-time GISAXS measurement on P3HT:PCBM solar cell devices illuminated with AM1.5 conditions done by Schaffer et al.[56] Khelifi et al. reported as well that the long-term degradation is caused by a change in the blend morphology evident by transmission electron microscopy (TEM) experiments.[62] As a result, the alternation of the nanomorphology of the active layer due to solar irradiation is mainly responsible for the degradation of the polymer solar cells in our study.

Since for organic photovoltaic devices, a preferred crystal orientation and a high crystallinity of the active layer are of great importance, both are probed with GIWAXS. Samples illuminated with AM0 for different times from 0 to 1800 s are measured with GIWAXS. By performing horizontal and vertical sector integrals from the 2D GIWAXS data, information about the crystal orientations, lattice constants, and crystal sizes is extracted. The probed Bragg peaks are fitted with Gaussian functions to identify the peak position and full width half maximum.[63,64] The corresponding horizontal and vertical sector integrals are presented in Figure 7. In the horizontal

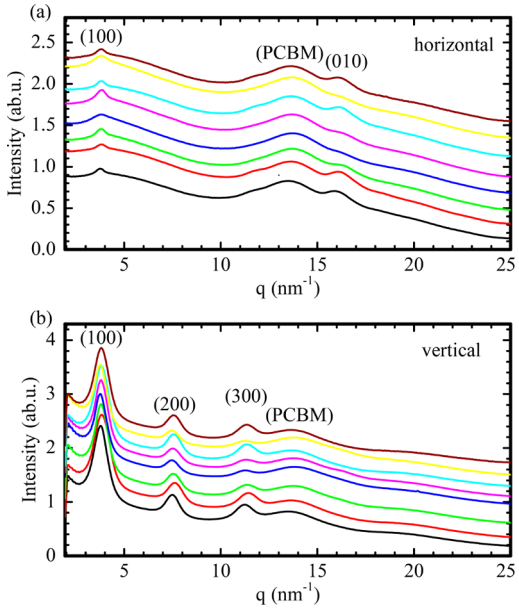

Figure 7. (a) Horizontal and (b) vertical sector integrals of 2D GIWAXS data measured for P3HT:$PC_{61}BM$ films illuminated with 1.0 AM0 for different illumination times at a constant temperature of 28 °C. From the bottom to the top, the illumination time increases from 0 to 1800 s. Characteristic features in the data are assigned to P3HT and PCBM as indicated.

sector integrals (see Figure 7a), both P3HT (100) and (010) Bragg reflections are visible for all probed illumination times. Moreover, the isotropically distributed PCBM also gives rise to a scattering signal at a position $q \sim 14$ nm^{-1}. From the vertical sector integrals, the appearance of higher order (200) and (300) Bragg peaks as well as more pronounced (100) Bragg peaks as compared with the horizontal direction illustrate the prevailing edge-on orientation in P3HT domains.

The numbers from the quantitative analysis of the GIWAXS data are given in Table 1. The lattice constant of P3HT along

Table 1. Lattice Constants and Crystal Sizes of P3HT Obtained from Sector Integrals of GIWAXS Measurements

	lattice constant (nm)			crystal size (nm)		
illumination time (s)	(100) v	(100) h	(010) h	(100) v	(100) h	(010) h
1	1.67	1.67	0.39	13.4	12.8	6.2
120	1.64	1.64	0.39	11.6	13.7	5.9
300	1.65	1.65	0.39	14.3	15.0	6.1
600	1.67	1.64	0.39	14.6	14.0	-
900	1.66	1.64	0.39	14.0	11.8	4.7
1200	1.65	1.65	0.39	12.8	13.4	5.6
1500	1.67	1.65	0.39	15.0	8.3	-
1800	1.64	1.65	0.39	12.1	12.6	5.1

the (100) direction is about 1.65 nm for both vertical and horizontal data, irrespective of illumination duration. Thus, illumination does not alter the polymer side-chain spacing in the investigated time range. Additionally, no changes occur to the polymer $\pi-\pi$ stacking distance, as a constant value of 0.39 nm is observed along the (010) direction. The crystal size for P3HT is obtained by applying the Scherrer equation.[65,66] It turns out that the crystal size of P3HT for both (100) and (010) directions also remains rather constant without significant changes during illumination.

The results of our GIWAXS measurements are consistent with work by Li and Yang, who investigated illumination-dependent changes in absorption curves using AM1.5 radiation and concluded that the degradation phenomenon is not caused by polymer crystallinity and/or reduced light absorption,[67] although the crystalline nanostructure of P3HT is highly responsible for the solar cell performance.[68] Similar observations were made by Kumar et al. by looking into absorption peaks arising from P3HT.[69]

4. CONCLUSION

In the present investigation we probe the performance and morphological evolution of P3HT:$PC_{61}BM$ BHJ solar cells under AM0 radiation conditions. Whereas terrestrial applications of polymer solar cells have been primarily investigated such information for AM1.5 radiation under different atmospheres (including normal conditions), our selection of testing parameters was inspired by space applications. The key parameters which describe the function of a polymer solar cell, that is, V_{oc}, I_{sc}, FF, and power conversion efficiency η, exhibit a strong dependence on solar intensity, temperature, and illumination time. The observed dependence of solar intensities is promising, as V_{oc} and I_{sc} are found to increase. Surprisingly, polymer solar cells still function very well under very harsh UV intensity of 3 AM0 solar spectrum. The identified temperature dependence is very promising, since device performance improves with increasing temperature, which rules out the need for active cooling when it comes to solar panel applications. Aging of course will be a key issue as in solar applications an exchange of solar device cannot be easily realized. In our initial experiments we have only focused on short-time aging, which is found to already limit device performance. From the GISAXS investigations it is mainly seen

that morphological changes occur on the mesoscale. These changes in domain sizes and distance are causing the decreasing device performance. As a result, it will become necessary to better stabilize the active layer morphology before looking with more detail into the long-term degradation related to conditions suited for space applications.

To the authors' knowledge, so far there are only a few in-depth investigations on the possibilities and potential of polymer solar cells being used in space applications. Our observations using AM0 solar spectrum do well coincide with the commonly performed work using AM1.5 radiation. However, to what extend a generalization based on the probed P3HT:$PC_{61}BM$ system can be done remains open. Further investigations regarding the influence of the extremely low temperature and the high-energy particles in space on the performance of polymer-based solar cells are undergoing. Nevertheless, in our opinion our results give clear evidence of a high potential for the usage of polymer solar cells for space applications.

AUTHOR INFORMATION

Corresponding Author

*Fax: +49 (0)89 289 12473. Tel.: +49 (0)89 289 12451. E-mail: muellerb@ph.tum.de.

Author Contributions

All authors have given approval to the final version of the manuscript.

Notes

The authors declare no competing financial interest.

ACKNOWLEDGMENTS

SG. is thankful for the financial support by the GreenTech Initiative (Interface Science for Photovoltaics—ISPV) of the EuroTech Universities together with TUM.solar in the frame of the Bavarian Collaborative Research Project "Solar Technologies go Hybrid" (SolTec). W.W. is thankful for the funding of CSC (China Scholarship Council). Part of this research was carried out at the synchrotron light sources DORISIII at DESY. DESY is a member of the Helmholtz Association (HGF). The authors thank Helmut Janker from Airbus Defense and Space for his technical assistance.

REFERENCES

(1) Rivnay, J.; Mannsfeld, S. C. B.; Miller, C. E.; Salleo, A.; Toney, M. F. Quantitative Determination of Organic Semiconductor Microstructure from the Molecular to Device Scale. *Chem. Rev.* **2012**, *112*, 5488−5519.

(2) An, Q.; Zhang, F.; Zhang, J.; Tang, W.; Wang, Z.; Li, L.; Xu, Z.; Teng, F.; Wang, Y. Enhanced Performance of Polymer Solar Cells through Sensitization by a Narrow Band Gap Polymer. *Sol. Energy Mater. Sol. Cells* **2013**, *118*, 30−35.

(3) Lipomi, D. J.; Tee, B. C. K.; Vosgueritchian, M.; Bao, Z. Stretchable Organic Solar Cells. *Adv. Mater.* **2011**, *23*, 1771−1775.

(4) Lee, M. R.; Eckert, R. D.; Forberich, K.; Dennler, G.; Brabec, C. J.; Gaudiana, R. A. Solar Power Wires Based on Organic Photovoltaic Materials. *Science* **2009**, *324*, 232−235.

(5) Oklobia, O.; Shafai, T. S. A Quantitative Study of the Formation of PCBM Clusters upon Thermal Annealing of P3HT/PCBM Bulk Heterojunction Solar Cell. *Sol. Energy Mater. Sol. Cells* **2013**, *117*, 1−8.

(6) Li, X.-G.; Li, J.; Meng, Q.-K.; Huang, M.-R. Interfacial Synthesis and Widely Controllable Conductivity of Polythiophene Microparticles. *J. Phys. Chem. B* **2009**, *113*, 9718−9727.

(7) Li, X.-G.; Huang, M.-R.; Duan, W.; Yang, Y.-L. Novel Multifunctional Polymers from Aromatic Diamines by Oxidative Polymerizations. *Chem. Rev.* **2002**, *102*, 2925−3030.

(8) Martín-Fabiani, I.; Siegel, J.; Riedel, S.; Boneberg, J.; Ezquerra, T. A.; Nogales, A. Nanostructuring Thin Polymer Films with Optical Near Fields. *ACS Appl. Mater. Interfaces* **2013**, *5*, 11402−11408.

(9) Guo, C.; Lin, Y.-H.; Witman, M. D.; Smith, K. A.; Wang, C.; Hexemer, A.; Strzalka, J.; Gomez, E. D.; Verduzco, R. Conjugated Block Copolymer Photovoltaics with Near 3% Efficiency through Microphase Separation. *Nano Lett.* **2013**, *13*, 2957−2963.

(10) Kesava, S. V.; Fei, Z.; Rimshaw, A. D.; Wang, C.; Hexemer, A.; Asbury, J. B.; Heeney, M.; Gomez, E. D. Domain Compositions and Fullerene Aggregation Govern Charge Photogeneration in Polymer/Fullerene Solar Cells. *Adv. Energy Mater.* **2014**, *4*, 1400116.

(11) Herzig, E. M.; Müller-Buschbaum, P. Organic Photovoltaic Cells for Space Applications. *Acta Futura* **2013**, *6*, 17−24.

(12) Kumar, A.; Rosen, N.; Devine, R.; Yang, Y. Interface Design To Improve Stability of Polymer Solar Cells for Potential Space Applications. *Energy Environ. Sci.* **2011**, *4*, 4917−4920.

(13) Otte, K.; Makhova, L.; Braun, A.; Konovalov, I. Flexible Cu(In,Ga)Se_2 Thin-Film Solar Cells for Space Application. *Thin Solid Films* **2006**, *511*, 613−622.

(14) Kumar, A.; Devine, R.; Mayberry, C.; Lei, B.; Li, G.; Yang, Y. Origin of Radiation-Induced Degradation in Polymer Solar Cells. *Adv. Funct. Mater.* **2010**, *20*, 2729−2736.

(15) Scharber, M. C.; Sariciftci, N. S. Efficienicy of Bulk-Heterojunction Organic Solar Cells. *Prog. Polym. Sci.* **2013**, *38*, 1929−1940.

(16) Nelson, J. Polymer:Fullerene Bulk Heterojunction Solar Cells. *Mater. Today* **2011**, *14*, 462−470.

(17) Yamaguchi, M.; Takamoto, T.; Khan, A.; Imaizumi, M.; Matsuda, S.; Ekins-Daukes, N. J. Super-High-Efficiency Multi-Junction Solar Cells. *Prog. Photovoltaics: Res. Appl.* **2005**, *13*, 125−132.

(18) Wu, J.; Walukiewicz, W.; Yu, K. M.; Shan, W.; Ager, J. W., III; Haller, E. E.; Lu, H.; Schaff, W. J.; Metzger, W. K.; Kurtz, S. Superior Radiation Resistance of In1−*x*Ga*x*N Alloys: Full-Solar-Spectrum Photovoltaic Material System. *J. Appl. Phys.* **2003**, *94*, 6477−6482.

(19) Dang, M. T.; Hirsch, L.; Wantz, G. P3HT:PCBM, Best Seller in Polymer Photovoltaic Research. *Adv. Mater.* **2011**, *23*, 3597−3602.

(20) Dennler, G.; Scharber, M. C.; Ameri, T.; Denk, P.; Forberich, K.; Waldauf, C.; Brabec, C. J. Design Rules for Donors in Bulk-Heterojunction Tandem Solar Cells—Towards 15% Energy-Conversion Efficiency. *Adv. Mater.* **2008**, *20*, 579−583.

(21) Ruderer, M. A.; Müller-Buschbaum, P. Morphology of Polymer-Based Bulk Heterojunction Films for Oganic Photovoltaics. *Soft Matter* **2011**, *7*, 5482−5493.

(22) Moungthai, S.; Mahadevapuram, N.; Ruchhoeft, P.; Stein, G. E. Direct Patterning of Conductive Polymer Domains for Photovoltaic Devices. *ACS Appl. Mater. Interfaces* **2012**, *4*, 4015−4023.

(23) Gevaerts, V. S.; Koster, L. J. A.; Wienk, M. M.; Janssen, R. A. J. Discriminating between Bilayer and Bulk Heterojunction Polymer:-Fullerene Solar Cells Using the External Quantum Efficiency. *ACS Appl. Mater. Interfaces* **2011**, *3*, 3252−3255.

(24) Clark, M. D.; Jespersen, M. L.; Patel, R. J.; Leever, B. J. Predicting Vertical Phase Segregation in Polymer−Fullerene Bulk Heterojunction Solar Cells by Free Energy Analysis. *ACS Appl. Mater. Interfaces* **2013**, *5*, 4799−4807.

(25) Müller-Buschbaum, P. In *Applications of Synchrotron Light to Scattering and Diffraction in Materials and Life Sciences*; Ezquerra, T. A., Garcia-Gutierrez, M. C., Nogales, A., Gomez, M., Eds.; Springer: Berlin, Heidelberg, 2009; Chapter 3, pp 61−86.

(26) Huang, Y.-C.; Tsao, C.-S.; Chuang, C.-M.; Lee, C.-H.; Hsu, F.-H.; Cha, H.-C.; Chen, C.-Y.; Lin, T.-H.; Su, C.-J.; Jeng, U.-S.; Su, W.-F. Small- and Wide-Angle X-ray Scattering Characterization of Bulk Heterojunction Polymer Solar Cells with Different Fullerene Derivatives. *J. Phys. Chem. C* **2012**, *116*, 10238−10244.

(27) Kaune, G.; Metwalli, E.; Meier, R.; Körstgens, V.; Schlage, K.; Couet, S.; Röhlsberger, R.; Roth, S. V.; Müller-Buschbaum, P. Growth

and Morphology of Sputtered Aluminum Thin Films on P3HT Surfaces. *ACS Appl. Mater. Interfaces* **2011**, *3*, 1055−1062.
(28) Perlich, J.; Memesa, M.; Diethert, A.; Metwalli, E.; Wang, W.; Roth, S. V.; Timmann, A.; Gutmann, J. S.; Müller-Buschbaum, P. Preservation of the Morphology of a Self-Encapsulated Thin Titania Film in a Functional Multilayer Stack: An X-ray Scattering Study. *ChemPhysChem* **2009**, *10*, 799−805.
(29) Li, X.-G.; Huang, M.-R. X-ray Diffraction of Thermotropic Liquid-Crystalline Copoly(Vanillate-4-Hydroxybenzoate-Ethyleneterephthalate). *Angew. Makromol. Chem.* **1997**, *249*, 93−114.
(30) Ruderer, M. A.; Guo, S.; Meier, R.; Chiang, H.-Y.; Körstgens, V.; Wiedersich, J.; Perlich, J.; Roth, S. V.; Müller-Buschbaum, P. Solvent Induced Morphology in Polymer-Based Systems for Organic Photovoltaics. *Adv. Funct. Mater.* **2011**, *21*, 3382−3391.
(31) Ruderer, M. A.; Prams, S. M.; Rawolle, M.; Zhong, Q.; Perlich, J.; Roth, S. V.; Müller-Buschbaum, P. Influence of Annealing and Blending of Photoactive Polymers on Their Crystalline Structure. *J. Phys. Chem. B* **2010**, *114*, 15451−15458.
(32) Kohn, P.; Huettner, S.; Komber, H.; Senkovskyy, V.; Tkachov, R.; Kiriy, A.; Friend, R. H.; Steiner, U.; Huck, W. T. S.; Sommer, J.; Sommer, M. On the Role of Single Regiodefects and Polydispersity in Regioregular Poly(3-hexylthiophene): Defect Distribution, Synthesis of Defect-Free Chains, and a Simple Model for the Determination of Crystallinity. *J. Am. Chem. Soc.* **2012**, *134*, 4790−4805.
(33) Guo, S.; Ruderer, M. A.; Rawolle, M.; Körstgens, V.; Birkenstock, C.; Perlich, J.; Müller-Buschbaum, P. Evolution of Lateral Structures during the Functional Stack Build-up of P3HT:PCBM-Based Bulk Heterojunction Solar Cells. *ACS Appl. Mater. Interfaces* **2013**, *5*, 8581−8590.
(34) Perlich, J.; Rubeck, J.; Botta, S.; Gehrke, R.; Roth, S. V.; Ruderer, M. A.; Prams, S. M.; Rawolle, M.; Zhong, Q.; Körstgens, V.; et al. Grazing Incidence Wide Angle X-ray Scattering at the Wiggler Beamline BW4 of HASYLAB. *Rev. Sci. Instrum.* **2010**, *81*, 105105−1−105105−7.
(35) Müller-Buschbaum, P. Grazing Incidence Small-Angle X-ray Scattering: An Advanced Scattering Technique for the Investigation of Nanostructured Polymer Films. *Anal. Bioanal. Chem.* **2003**, *376*, 3−10.
(36) Park, Y.; Noh, S.; Lee, D.; Kim, J. Y.; Lee, C. Temperature and Light Intensity Dependence of Polymer Solar Cells with MoO_3 and PEDOT: PSS as a Buffer Layer. *J. Korean Phys. Soc.* **2011**, *59*, 362−366.
(37) Riedel, I.; Parisi, J.; Dyakonov, V.; Lutsen, L.; Vanderzande, D.; Hummelen, J. C. Effect of Temperature and Illumination on the Electrical Characteristics of Polymer−Fullerene Bulk-Heterojunction Solar Cells. *Adv. Funct. Mater.* **2004**, *14*, 38−43.
(38) Tromholt, T.; Madsen, M. V.; Krebs, F. C. Ultra High Open Circuit Voltage (>1 V) of Poly-3-hexylthiophene Based Organic Solar Cells with Concentrated Light. *Appl. Phys. Lett.* **2013**, *102*, 123904−123908.
(39) Katz, E. A.; Manor, A.; Mescheloff, A.; Tromholt, T.; Krebs, F. C. Accelerated Stability Testing of Organic Photovoltaics Using Concentrated Sunlight. *Conference record of the IEEE Photovoltaic Specialists Conference*; IEEE, Austin, TX, 2012; pp 003249−003252.
(40) Madsen, M. V.; Tromholt, T.; Norrman, K.; Krebs, F. C. Concentrated Light for Accelerated Photo Degradation of Polymer Materials. *Adv. Energy Mater.* **2013**, *3*, 424−427.
(41) Koster, L. J. A.; Mihailetchi, V. D.; Ramaker, R.; Blom, P. W. M. Light Intensity Dependence of Open-Circuit Voltage of Polymer:-Fullerene Solar Cells. *Appl. Phys. Lett.* **2005**, *86*, 123509−1−123509−3.
(42) Tromholt, T.; Katz, E. A.; Hirsch, B.; Vossier, A.; Krebs, F. C. Effects of Concentrated Sunlight on Organic Photovoltaics. *Appl. Phys. Lett.* **2010**, *96*, 073501−1−073501−3.
(43) Khan, F.; Singh, S. N.; Husain, M. Effect of Illumination Intensity on Cell Parameters of A Silicon Solar Cell. *Sol. Energy Mater. Sol. Cells* **2010**, *94*, 1473−1476.
(44) Katz, E. A.; Faiman, D.; Tuladhar, S. M. Temperature Dependence for the Photovoltaic Device Parameters of Polymer−Fullerene Solar Cells under Operating Conditions. *J. Appl. Phys.* **2001**, *90*, 5343−5350.
(45) Bässler, H. Charge Transport in Disordered Organic Photoconductors a Monte Carlo Simulation Study. *Phys. Status Solidi B* **1993**, *175*, 15−56.
(46) Mihailetchi, V. D.; van Duren, J. K. J.; Blom, P. W. M.; Hummelen, J. C.; Janssen, R. A. J.; Kroon, J. M.; Rispens, M. T.; Verhees, W. J. H.; Wienk, M. M. Electron Transport in a Methanofullerene. *Adv. Funct. Mater.* **2003**, *13*, 43−46.
(47) Chirvase, D.; Chiguvare, Z.; Knipper, M.; Parisi, J.; Dyakonov, V.; Hummelen, J. C. Temperature Dependent Characteristics of Poly(3 hexylthiophene)−Fullerene Based Heterojunction Organic Solar Cells. *J. Appl. Phys.* **2003**, *93*, 3376−3383.
(48) Yazawa, K.; Inoue, Y. Twist Glass Transition in Regioregulated Poly(3-alkylthiophene)s. *Phys. Rev. B* **2006**, *74*, 094204−1−094204−12.
(49) Peters, C. H.; Sachs-Quintana, I. T.; Mateker, W. R.; Heumueller, T.; Rivnay, J.; Noriega, R.; Beiley, Z. M.; Hoke, E. T.; Salleo, A.; McGehee, M. D. The Mechanism of Burn-in Loss in a High Efficiency Polymer Solar Cells. *Adv. Mater.* **2012**, *24*, 663−668.
(50) Singh, P.; Ravindra, N. M. Temperature Dependence of Solar Cell Performance—An Analysis. *Sol. Energy Mater. Sol. Cells* **2012**, *101*, 36−45.
(51) Tipnis, R.; Bernkopf, J.; Jia, S.; Krieg, J.; Li, S.; Storch, M.; Laird, D. Large-Area Organic Photovoltaic Module—Fabrication and Performance. *Sol. Energy Mater. Sol. Cells* **2009**, *93*, 442−446.
(52) Agbomahena, M.; Douhéret, O.; Kounouhewa, B.; Vianou, A.; Awanou, N.; Lazzaroni, R. Aging of Organic Photovoltaic Devices in Benin Environment (South-Sudanese Climate). *Sol. Energy Mater. Sol. Cells* **2013**, *117*, 93−97.
(53) Bertho, S.; Janssen, G.; Cleij, T. J.; Conings, B.; Moons, W.; Gadisa, A.; D'Haen, J.; Goovaerts, E.; Lutsen, L.; Manca, J.; Vanderzande, D. Effect of Temperature on the Morphological and Photovoltaic Stability of Bulk Heterojunction Polymer:Fullerene Solar Cells. *Sol. Energy Mater. Sol. Cells* **2008**, *92*, 753−760.
(54) Tromholt, T.; Manceau, M.; Helgesen, M.; Carlé, J. E.; Krebs, F. C. Degradation of Semiconducting Polymers by Concentrated Sunlight. *Sol. Energy Mater. Sol. Cells* **2011**, *95*, 1308−1314.
(55) Norrman, K.; Krebs, F. C. Lifetimes of Organic Photovoltaics: Combining Chemical and Physical Characterisation Techniques To Study Degradation Mechanisms. *Sol. Energy Mater. Sol. Cells* **2006**, *90*, 2793−2814.
(56) Schaffer, C. J.; Palumbiny, C. M.; Niedermeier, M. A.; Jendrzejewski, C.; Santoro, G.; Roth, S. V.; Müller-Buschbaum, P. A Direct Evidence of Morphological Degradation on a Nanometer Scale in Polymer Solar Cells. P. *Adv. Mater.* **2013**, *25*, 6760−6764.
(57) Jørgensen, M.; Norrman, K.; Krebs, F. C. Stability/Degradation of Polymer Solar Cells. *Sol. Energy Mater. Sol. Cells* **2008**, *92*, 686−714.
(58) Wang, X.; Zhao, C. X.; Xu, G.; Chen, Z.-K.; Zhu, F. Degradation Mechanisms in Organic Solar Cells: Localized Moisture Encroachment and Cathode Reaction. *Sol. Energy Mater. Sol. Cells* **2012**, *104*, 1−6.
(59) Peters, C. H.; Sachs-Quintana, I. T.; Kastrop, J. P.; Beaupré, S.; Leclerc, M.; McGehee, M. D. High Efficiency Polymer Solar Cells with Long Operating Lifetimes. *Adv. Energy Mater.* **2011**, *1*, 491−494.
(60) Tanenbaum, D. M.; Hermenau, M.; Voroshazi, E.; Lloyd, M. T.; Galagan, Y.; Zimmermann, B.; Hösel, M.; Dam, H. F.; Jørgensen, M.; Gevorgyan, S. A.; et al. The ISOS-3 Interlaboratory Collaboration Focused on the Stability of a Variety of Organic Photovoltaic Devices. *RSC Adv.* **2012**, *2*, 882−893.
(61) Chen, C.-Y.; Tsao, C.-S.; Huang, Y.-C.; Liu, H.-W.; Chiu, W.-Y.; Chuang, C.-M.; Jeng, U.-S.; Su, C.-J.; Wu, W.-R.; Su, W.-F.; Wang, L. Mechanism and Control of the Structural Evolution of a Polymer Solar Cell from Bulk Heterojunction to a Thermally Unstable Hierarchical Structure. *Nanoscale* **2013**, *5*, 7629−7638.
(62) Khelifi, S.; Voroshazi, E.; Spoltore, D.; Piersimoni, F.; Bertho, S.; Aernouts, T.; Manca, J.; Lauwaert, J.; Vrielinck, H.; Burgelman, M. Effect of Light Induced Degradation on Electrical Transport and Charge Extraction in Polythiophene:Fullerene (P3HT:PCBM) Solar Cells. *Sol. Energy Mater. Sol. Cells* **2014**, *120*, 244−252.

(63) Verploegen, E.; Mondal, R.; Bettinger, C. J.; Sok, S.; Toney, M. F.; Bao, Z. Effects of Thermal Annealing upon the Morphology of Polymer−Fullerene Blends. *Adv. Funct. Mater.* **2010**, *20*, 3519−3529.
(64) Guo, S.; Herzig, E.; Naumann, A.; Tainter, G.; Perlich, J.; Müller-Buschbaum, P. Influence of Solvent and Solvent Additive on the Morphology of PTB7 Films Probed via X-ray Scattering. *J. Phys. Chem. B* **2014**, *118*, 344−350.
(65) Monshi, A.; Foroughi, M. R.; Monshi, M. R. Modified Scherrer Equation To Estimate More Accurately Nano-Crystallite Size Using XRD. *World J. Nanosci. Eng.* **2012**, *2*, 154−160.
(66) Smilgies, D.-M. Scherrer Grain-Size Analysis Adapted to Grazing-Incidence Scattering with Area Detectors. *J. Appl. Crystallogr.* **2009**, *42*, 1030−1034.
(67) Li, G.; Yang, Y. Radiation Induced Damage and Recovery in Poly(3-hexyl thiophene) Based Polymer Solar Cells. *Nanotechnology* **2008**, *19*, 424014−1−424014−4.
(68) Chu, C. W.; Yang, H.; Hou, W. J.; Huang, J.; Li, G.; Yang, Y. Control of the Nanoscale Crystallinity and Phase Separation in Polymer Solar Cells. *Appl. Phys. Lett.* **2008**, *92*, 103306−103310.
(69) Kumar, A.; Hong, Z.; Sista, S.; Yang, Y. The Critical Role of Processing and Morphology in Determining Degradation Rates in Polymer Solar Cells. *Adv. Energy Mater.* **2011**, *1*, 124−131.